

A new type of high efficiency with a lowcost solar cell having the structure of a μSiC /polycrystalline silicon heterojunction

Y. Matsumoto, G. Hirata, H. Takakura, H. Okamoto, and Y. Hamakawa

Citation: *J. Appl. Phys.* **67**, 6538 (1990); doi: 10.1063/1.345131

View online: <http://dx.doi.org/10.1063/1.345131>

View Table of Contents: <http://jap.aip.org/resource/1/JAPIAU/v67/i10>

Published by the [American Institute of Physics](#).

Related Articles

Temperature-dependent transport and transient photovoltaic properties of $\text{La}_{2/3}\text{Ca}_{1/3}\text{MnO}_3/\text{Nb:SrTiO}_3$ heteroepitaxial p-n junction

J. Appl. Phys. **112**, 023101 (2012)

Investigation of deep-level defects in conductive polymer on n-type 4H- and 6H-silicon carbide substrates using I-V and deep level transient spectroscopy techniques

J. Appl. Phys. **112**, 014505 (2012)

Hole transport in pure and doped hematite

J. Appl. Phys. **112**, 013701 (2012)

Single GaInP nanowire p-i-n junctions near the direct to indirect bandgap crossover point

Appl. Phys. Lett. **100**, 251103 (2012)

Modeling charge transfer at organic donor-acceptor semiconductor interfaces

APL: Org. Electron. Photonics **5**, 109 (2012)

Additional information on *J. Appl. Phys.*


Journal Homepage: <http://jap.aip.org/>

Journal Information: http://jap.aip.org/about/about_the_journal

Top downloads: http://jap.aip.org/features/most_downloaded

Information for Authors: <http://jap.aip.org/authors>

ADVERTISEMENT



AIP Advances

Special Topic Section:
PHYSICS OF CANCER

Why cancer? Why physics? [View Articles Now](#)

A new type of high efficiency with a low-cost solar cell having the structure of a $\mu\text{c-SiC}$ /polycrystalline silicon heterojunction

Y. Matsumoto, G. Hirata, H. Takakura, H. Okamoto, and Y. Hamakawa
Faculty of Engineering Science, Osaka University, Toyonaka, Osaka 560, Japan

(Received 15 January 1990; accepted for publication 6 February 1990)

A new type of high-efficiency solar cell has been developed by a simple production process only with electron cyclotron resonance plasma-assisted chemical vapor deposition of highly conductive microcrystalline silicon carbide ($\mu\text{c-SiC}$) on polycrystalline silicon (poly-Si). The device consists of a p -type $\mu\text{c-SiC}/n$ -type poly-Si heterojunction where the window material is a specially made wide-band gap and highly conductive $\mu\text{c-SiC}$. At the present stage, a conversion efficiency of 15.4% with $V_{oc} = 556$ mV, $J_{sc} = 35.7$ mA/cm², and F. F. = 77.4% has been achieved. Also employing this device as a bottom cell in a four-terminal amorphous silicon (a -Si) tandem-type solar cell, 16.8% efficiency has been obtained. A series of technical data on the fabrication technology and device performance is presented and discussed.

I. INTRODUCTION

In the recent 10 years, remarkable progress has been seen in solar photovoltaic technology.¹ One of the most important key issues to success in this project is the development of high-efficiency and low-cost solar cells. With the aid of national and/or seminational projects motivated to develop renewable clean energy, wide varieties of research and development efforts have been made from photovoltaic materials to system technologies. Particular focus has been placed on amorphous silicon (a -Si) solar cells which have a potentiality to approach the aimed milestone. However, as is well known, the a -Si solar cell has a severe drawback in long-term stability, that is, a kind of light-induced degradation based upon the Staebler-Wronski effect.² To solve this problem, a series of basic researches have been carried out, for example, new film deposition technologies such as ultra-high-vacuum plasma-assisted chemical vapor deposition³ (UHV CVD), electron cyclotron resonance plasma-assisted chemical vapor deposition⁴ (ECR CVD), and also new device structures like tandem-type solar cells.⁵ By the use of ECR plasma CVD, we have recently succeeded in preparing a highly conductive wide-gap microcrystalline silicon carbide ($\mu\text{c-SiC}$).⁶ The optical gap can be increased up to 2.7 eV without any significant reduction in electrical conductivity.

The $\mu\text{c-SiC}$ has been applied to polycrystalline silicon (poly-Si) based heterojunction cells as a window electrode layer. The device is fabricated with a low-temperature process and consists of a very simple structure, while its performance is considerably good as compared with that of poly-Si solar cells fabricated by the conventional high-temperature diffusion process. This fact reveals the merit and usefulness of the ECR plasma deposition technique to the production sequence for low-cost, highly reliable solar cells. From this point of view, we have explored the possibility for higher efficiency on $\mu\text{c-SiC}/\text{poly-Si}$ stacked optically in series with an a -Si/ a -Si-based cell for the four-terminal tandem-type solar cell.

In this paper, the fabrication process and basic proper-

ties of ECR-plasma-produced $\mu\text{c-SiC}$ are first reported. Then, the device performances of $\mu\text{c-SiC}/\text{poly-Si}$ heterojunction cells as well as a -Si/poly-Si-based four-terminal devices are demonstrated in conjunction with their material, junction properties, and cell design parameters.

II. ECR PLASMA CVD SYSTEM AND DEPOSITION CONDITIONS

Figure 1(a) illustrates a schematic diagram of the ECR CVD apparatus employed in this work. Microwave power at

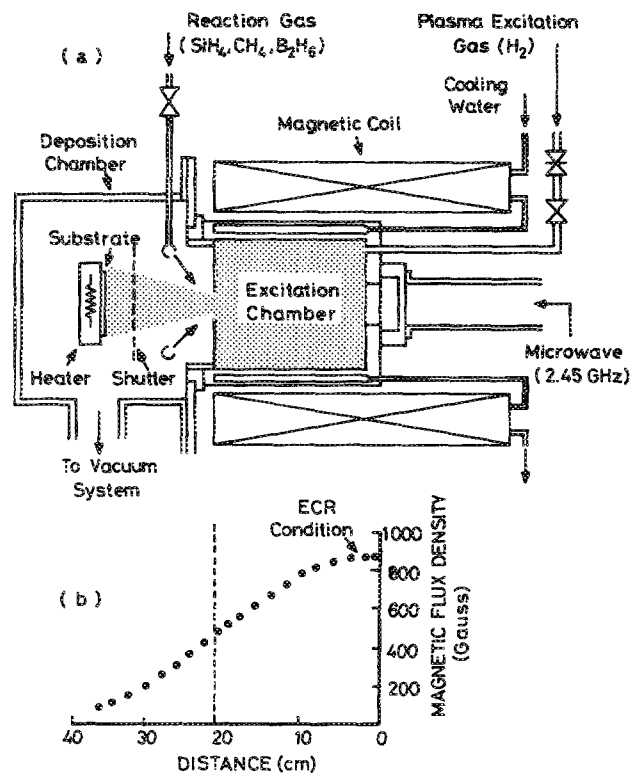


FIG. 1. (a) Schematic diagram of electron cyclotron resonance (ECR) plasma CVD system and (b) the profile of the magnetic field for the extraction of the plasma from the excitation chamber into the deposition chamber.

TABLE I. Preparation conditions of *p*- and *n*-type $\mu\text{c-SiC}$ by ECR plasma CVD.

Substrate temperature	250–350 °C
Microwave power	250–320 W
Total gas pressure	7×10^{-4} Torr
Plasma excitation gas (flow rate)	H_2 10–100 sccm
Reaction gas (flow rate)	SiH_4 (10% in H_2) 5–20 sccm CH_4 (10% in H_2) 5–30 sccm B_2H_6 (0.05% in H_2) 40–75 sccm PH_3 (0.05% in H_2) 40–80 sccm
Microwave frequency	2.45 GHz
Magnetic flux density	875 G

2.45 GHz is introduced into the ECR plasma excitation chamber through a rectangular waveguide and a window made of fused quartz plate. The ECR excitation chamber is a cylindrical resonator of TE_{113} mode, surrounded by a magnetic coil. In the system, the magnetic flux required for satisfying the electron cyclotron resonance condition is about 875 G. The ECR plasma is extracted from the ECR excitation chamber into the deposition chamber along with the gradient of dispersed magnetic field as is shown in Fig. 1(b). The extracted ECR plasma interacts with the reaction gas introduced into the deposition chamber to produce active species for film growth.

In the present experiment, hydrogen was used as an ECR plasma excitation gas, and a mixture of SiH_4 , CH_4 , B_2H_6 , and PH_3 was used as a reaction gas for the growth of *p*- and *n*-type $\mu\text{c-SiC}$.⁷ Details of the preparation conditions are summarized in Table I.

The unique feature of the ECR CVD is that the growing surface is subject to bombardment by electrons and/or other heavy species having a uniform and moderate energy of several tens of eV.⁸ This effect not only prevents weak bonds from being incorporated into the network, but also promotes diffusion of long-lifetime radical species into the film due to the raised surface temperature. It is expected that films with dense network and low defect density are formed. In the case of ECR CVD using hydrogen as an excitation gas, a large concentration of hydrogen radicals will arrive at the growing surface which drive out weakly bonded hydrogen at the surface and promote the formation of nonhydrogenated silicon-related microcrystallites. The existence of such microcrystalline phases are clearly confirmed by Raman spectra. Raman spectra of the films prepared with the growth conditions listed in the Table I exhibit distinct structures peaking at around 520 and 740 cm^{-1} , which corresponds to TO-phonon modes of crystalline Si and crystalline SiC clusters.⁶

III. ELECTRICAL AND OPTICAL PROPERTIES OF DOPED $\mu\text{c-SiC}$ FILMS

The optical energy gap of prepared samples were determined in accordance with Tauc's model of optical absorption.⁹ Figure 2 shows the relation between the dark conductivity and the optical energy gap of both *p*- and *n*-type $\mu\text{c-SiC:H}$ prepared by ECR plasma CVD. Similar plots are also given for *p*- and *n*-type *a-SiC:H* prepared by convention-

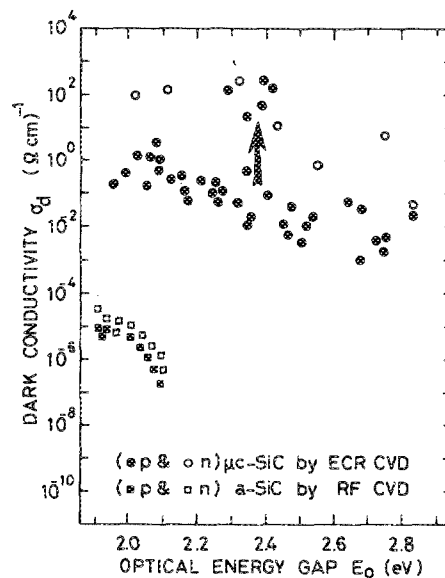


FIG. 2. Plots of dark conductivity σ_d for boron- and phosphorus-doped $\mu\text{c-SiC}$ film prepared with ECR CVD as a function of its optical energy gap. Filled (open) circle plots express the *p*-type (*n*-type) $\mu\text{c-SiC}$ prepared at constant substrate temperature of 300 °C with hydrogen gas dilution ratio $\text{H}_2/(\text{SiH}_4 + \text{CH}_4)$ of 35–65, and boron (phosphorus) doping ratio of 0.75%–1.25%. The rf-produced *a-SiC* is also shown with square plots.

al radio frequency (rf) plasma CVD. The band gap was controlled by adjusting the fraction of CH_4/SiH_4 in the reaction gas. The greater CH_4/SiH_4 ratio implies increments of optical energy gap, but the dark conductivity of the films prepared by the rf plasma CVD drastically decreases, while that of the films prepared by the ECR plasma CVD remains higher than $10^{-3} \text{ S cm}^{-1}$, even when the optical energy gap exceeds 2.7 eV. Hall measurement of boron-doped $\mu\text{c-SiC}$ material with a 2.25-eV optical gap has revealed *p*-type conduction with a hole mobility of around $1.2 \text{ cm}^2 \text{ V}^{-1} \text{ s}^{-1}$ and carrier concentration in the order of 10^{18} cm^{-3} . A higher hydrogen dilution of the reaction gas during the deposition leads to a marked enhancement in the conductivity as is indicated by the arrow in Fig. 2. This increase is primarily due to the increment in mobility, reaching about $20 \text{ cm}^2 \text{ V}^{-1} \text{ s}^{-1}$.¹⁰

Figure 3 shows the optical absorption spectra of several *p*-type SiC films prepared by ECR plasma CVD (solid lines) and conventional rf plasma CVD (broken line). The closed circle on each curve indicates the position of the optical band gap determined by Tauc's procedure. As can be seen in the figure, the absorption coefficient spectra of $\mu\text{c-SiC}$ films shift towards the short-wavelength side as the optical band gap increases from 2.1 to 2.7 eV. Since the electronic states involved in optical transition might have different characters for amorphous and microcrystalline materials, Tauc's optical band gap does not offer a direct measure of the absorption coefficient or the optical transparency. Indeed, the absorption coefficient of 2.1-eV band-gap $\mu\text{c-SiC}$ is larger than that of 2.0-eV band-gap *a-SiC* in almost entire spectral region covered in this measurement. Thus, as far as the optical transparency required for the heterojunction window layer

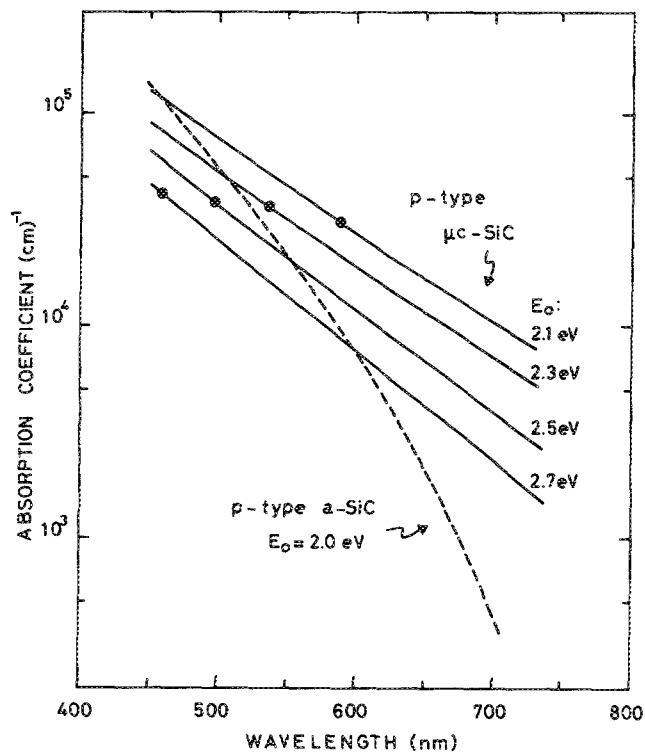


FIG. 3. Absorption coefficient spectra of *p*-type $\mu\text{c-SiC}$ with various optical energy gaps (E_0) as a function of wavelength. The films were prepared with gas source condition of $\text{CH}_4/\text{SiH}_4 = 1-3$. The absorption spectra of *p*-type *a*-SiC is also indicated as a reference.

is concerned, the $\mu\text{c-SiC}$ with relatively low optical band gaps like 2.1 eV have no advantage over the conventional *a*-SiC. However, also found in the figure is that the 2.7-eV band-gap $\mu\text{c-SiC}$ is more optically transparent than 2.0-eV band-gap *a*-SiC in an appreciable spectral range of practical importance, indicating the usefulness of wide-gap $\mu\text{c-SiC}$ from both the optical and electrical aspects.

IV. $\mu\text{c-SiC}/\text{poly-Si}$ HETEROJUNCTION SOLAR CELL

A. Cell structure and fabrication process

Utilizing highly conductive *p-μc-SiC* film described in the former section, heterojunction solar cells of the structure $\mu\text{c-SiC}/\text{poly-Si}$ were fabricated. The material used as a base substrate was 2–4- Ω cm, 0.025-cm-thick *n*-type cast polycrystalline Si. As the first step of the cell fabrication, aluminum was deposited on the poly-Si substrate for taking a back ohmic contact. After the buffered HF surface treatment, a *p*-type $\mu\text{c-SiC}$ layer was deposited on this substrate by ECR plasma CVD to form a *p-n* heterojunction. Finally, indium thin oxide (ITO) of around 75 nm thick was deposited at a substrate temperature of 250 °C by the electron-beam deposition technique as an antireflecting coating and front electrode layer.

B. Heterojunction cell performance

Figure 4 shows the photovoltaic performances of heterojunction solar cells made with *p*-type $\mu\text{c-SiC}$ having various optical band gaps. The open-circuit voltage (V_{oc}) as well as

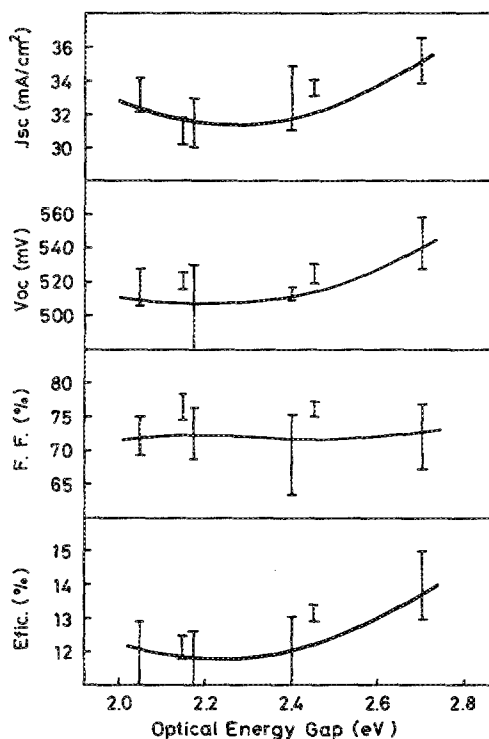


FIG. 4. Photovoltaic characteristics of *p-μc-SiC/n-poly-Si* heterojunction solar cell as a function of emitter layer optical band gap. The emitter thickness is approximately 70 nm in all devices.

short-circuit current (J_{sc}) tend to increase for a wider optical band-gap region. To understand this behavior, current-voltage (*I-V*) and capacitance-voltage (*C-V*) measurements were carried out on two representative solar cells. The cells denoted as a and b in Table II were prepared with a 70-nm-thick $\mu\text{c-SiC}$ emitter with 2.70- and 2.17-eV optical band gaps, respectively. The saturation current determined from an extrapolation of the dark *I-V* curve differs in one order of magnitude between the cells. The reason for a smaller saturation current of the wider band-gap cell is likely to be associated with the carbon interaction effects in the film growth process. The fraction of hydrocarbon may have a significant influence on the amount of hydrogen atoms incorporated into the deposited $\mu\text{c-Si}$ film; the hydrogen concentration increases with the amount of CH_4 .¹¹ This would result in an efficient hydrogen passivation at the emitter/base interface, decreasing the interface states which play a central role in determining the saturation current. On the other hand, *C-V* measurement made at 100 kHz reveals the increment of built-in potential (V_d) for the sample prepared with wider

TABLE II. Comparison of $\mu\text{c-SiC}/\text{poly-Si}$ heterojunction cells made with different emitter band gaps.

Cell	Emitter gap (eV)	Built-in potential (V)	Diode factor	J_0 (A/cm^2)
a	2.7	0.71	2.1	5×10^{-7}
b	2.1	0.63	1.9	4.2×10^{-6}

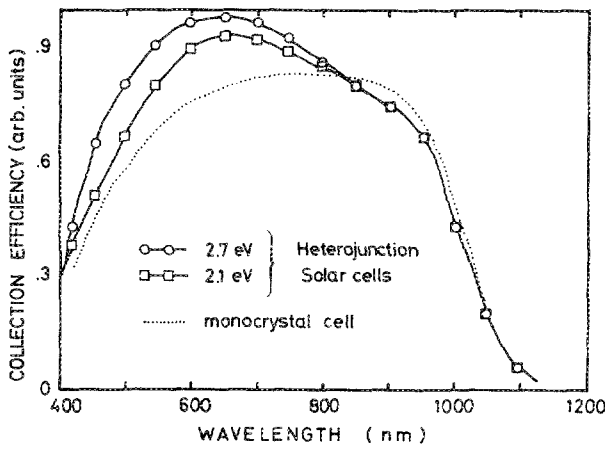


FIG. 5. Collection efficiency spectra of $\mu\text{c-SiC/poly-Si}$ heterojunction cells with different emitter band gaps. Open circles and squares refer to cells made with emitter optical band gaps of 2.7 and 2.17 eV, respectively. The dotted line indicates a monocrystal silicon cell fabricated by a conventional high-temperature process with approximately 400-nm junction depth.

band-gap material (see Table II). Both the factors mentioned above could explain the improvements of V_{oc} for wider emitter band-gap solar cells. The linear $1/C^2$ plots in the function of applied voltage indicate a step junction structure of the cell, and their slope fits well to the substrate impurity concentration.

Figure 5 shows the collection efficiency spectra of cells a and b which are listed in the Table II. The collection efficiency spectra of a p^+/n single-crystal silicon solar cell which was prepared with the conventional thermal process is also shown in this figure as a reference. The junction depth

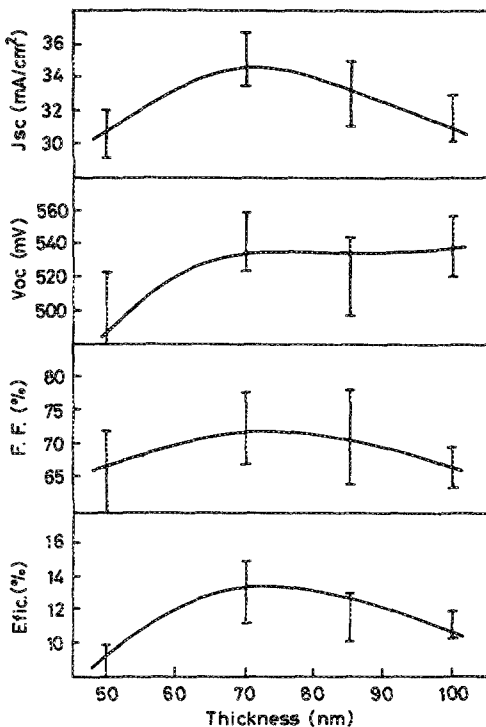


FIG. 6. Photovoltaic performances of the $\mu\text{c-SiC/poly-Si}$ heterojunction solar cell with 2.7-eV optical gap emitter as a function of its emitter thickness.

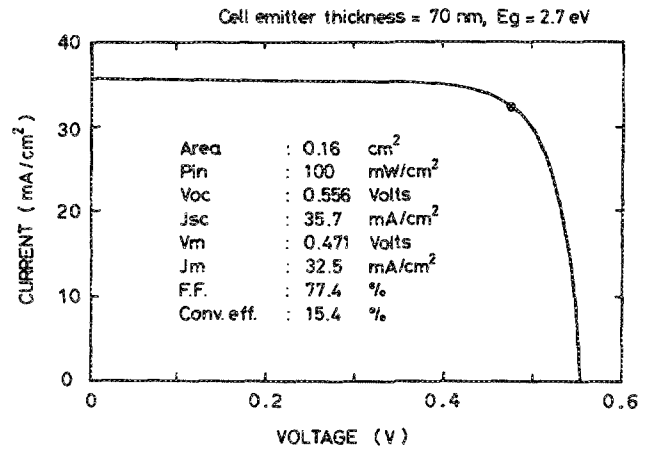


FIG. 7. Output characteristics of ITO/ $p\text{-}\mu\text{c-SiC/n-poly-Si/Al}$ heterojunction solar cell under AM1 solar simulated radiation of 100 mW/cm^2 at 25°C .

was approximately 400 nm. As can be seen, the $\mu\text{c-SiC/poly-Si}$ heterojunction cells exhibit an improved collection efficiency over the p^+/n monocrystal-Si cell in the short-wavelength region less than about 800 nm. Also the wider band-gap $\mu\text{c-SiC}$ window layer cell has better collection in this short spectral region, which is a natural consequence of the reduced absorption loss in the window emitter layer and corresponds to the variation of J_{sc} found in Fig. 4.

Photovoltaic performances of the cells also depend on the $\mu\text{c-SiC}$ emitter layer thickness as demonstrated in Fig. 6. As the emitter thickness is increased, the V_{oc} increases gradually and saturates at 100 nm, while the J_{sc} continuously decreases due to an increased absorption at the $\mu\text{c-SiC}$ emitter layer. Thus the optimum emitter thickness is found at around 70 nm for $\mu\text{c-SiC}$ with 2.7-eV optical band gap. Figure 7 shows the current-voltage characteristics of the heterojunction cell measured under simulated AM1 sunlight (100 mW/cm^2). The best conversion efficiency achieved is 15.4% with $V_{oc} = 556 \text{ mV}$, $J_{sc} = 35.7 \text{ mA/cm}^2$, and $\text{F.F.} = 77.4\%$. The high current density obtained is obviously due to the enhanced collection efficiency at higher photon energy region of the solar spectrum by the use of a wider band-gap emitter. The fill factor achieved also indicates the excellent quality of heterojunction formed with highly conductive microcrystalline silicon carbide.

V. FOUR-TERMINAL SOLAR CELL

A. Fabrication of $a\text{-Si}$ top cell

Utilizing the $\mu\text{c-SiC/poly-Si}$ heterojunction device described in the former section as a bottom cell, we also have developed a four-terminal $a\text{-Si/poly-Si}$ tandem-type solar cell, with structure as illustrated in Fig. 8.

The $a\text{-Si}$ top cell consists of a conventional $p\text{-}a\text{-SiC/i-a-Si/n-}\mu\text{c-Si}$ heterojunction. The amorphous and microcrystalline layers were prepared by the rf plasma deposition technique from a SiH_4/H_2 (1:9) mixture gas containing the desired amount of CH_4 , B_2H_6 , or PH_3 . Each layer was formed in a separate chamber to minimize the cross contamination effects. The layer thicknesses were 10 nm for p ,

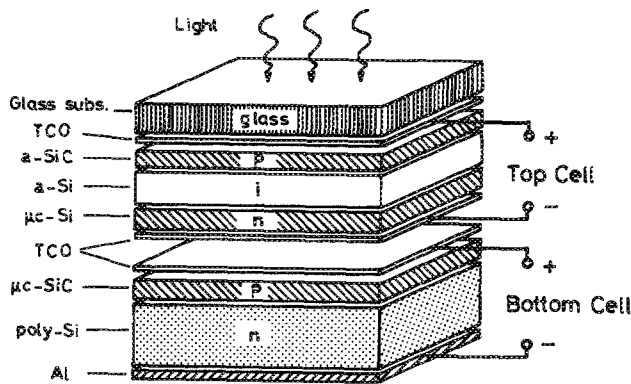


FIG. 8. Structure of *a*-Si/poly-Si four-terminal heterojunction tandem-type solar cell. The top cell consists of *a*-SiC/*a*-Si heterojunction materials and the bottom cell of μ c-SiC/poly-Si heterojunction cell.

400–500 nm for *i*, and 25 nm for *n* with a band gap of 1.89, 1.75, and 1.90 eV, respectively. The reaction gas source ratio for film preparation for *p*-*a*-SiC was $\text{SiH}_4:\text{CH}_4:\text{B}_2\text{H}_6 = 4:3:0.015$ and for *n*- μ c-Si $\text{SiH}_4:\text{H}_2:\text{PH}_3 = 2:60:0.01$ with a rf plasma power of 5 and 50 W, respectively. The substrate temperature during the deposition was 250 °C.

A series of solar cells has been fabricated on two kind of substrates. One is the glass/textured TCO (transparent conductive oxide) (660 nm thick, 12 Ω/\square), and the other was glass/smooth TCO (220 nm thick, 18 Ω/\square) with 5% and less than 1% haze, respectively. Finally, electron-beam-deposited ITO (about 70 nm thick) was provided for the back electrode contact. Also was fabricated a conventional cell with aluminum back contact for comparison. Output performances of the cells are listed in the Table III. The cell A1 denotes a conventional *p*-*a*-SiC/*i*-*a*-Si/*n*- μ c-Si heterojunction cell formed on a textured TCO glass substrate with nearly optimized conditions for the single-junction operation. Aluminum was used as a back contact in this cell, and it exhibits a conversion efficiency in excess of 10%. The cell A2

is optimized cell with an ITO back contact in the single-cell operation. The cell A3 was prepared on a smooth TCO substrate with less *i*-*a*-Si layer thickness.

B. Optimization of four-terminal device

The utilization of optical confinement effect with a textured TCO substrate is now a well-established technology for high-efficiency *a*-Si single-junction cells. However, if this technology is applied to the top cell of tandem devices, it inevitably reduces the amount of photons to be driven into the bottom cell. Figure 9 demonstrates how significant the effect is, where the portion of solar radiation transmitted through *a*-Si cells fabricated on textured [Fig. 9(a)] and smooth [Fig. 9(b)] TCO substrates are indicated by the shaded areas. Those sample structures are exactly the same as the cells A2 and A3 described in Table III. Figure 9 implies that the “optimized” condition for the single-cell operation does not always yield better results in the four-terminal device. Another concern here is the importance of optical connection between the bottom and top cells. The optical coupler minimizes loss due to the optical mismatching; otherwise, the net efficiency decreases by about 10% at least. We have employed silicon oil as a coupler in this experiment.

C. Four-terminal cell performance.

We have employed the best *p*- μ c-SiC/poly-Si cell described in Sec. IV as a bottom side of four-terminal tandem-type solar cell. The performances of each top and bottom solar cells and their combinations for tandem-type operation are also summarized in Table III.

The combination of A2 top cell and B2 bottom cell (B1 cell optically filtered with A2 cell) yields only 12% efficiency, which is substantially lower than the efficiency of bottom cell alone (B1). On the other hand, due to the lower value in short-circuit current density, the efficiency of A3 cell is inferior to A2 cell; however, the total efficiency of the tandem cell (A3 + B3) exhibits a remarkable improvement from that of the A2 + B2 combination, achieving the high-

TABLE III. *a*-Si/poly-Si, four-terminal tandem-type solar-cell performance.

Cell	V_{oc} (mV)	J_{sc} (mA/cm ²)	F.F. (%)	η (%)	Remarks
A1	842	17.6	68.8	10.2	Textured subs. + A1 (<i>i</i> layer = 500 nm)
A2	847	16.0	61.1	8.3	Textured subs. + ITO (<i>i</i> layer = 500 nm)
A3	867	13.4	61.0	7.1	Smooth subs. + ITO (<i>i</i> layer = 400 nm)
B1	556	35.7	77.4	15.4	Unfiltered
B2	516	11.2	75.1	4.3	Filtered with A2
B3	545	23.2	76.6	9.7	Filtered with A3
A2 + B2				12.6	8.3% + 4.3% (top) + (bottom)
A3 + B3				16.8	7.1% + 9.7% (top) + (bottom)

Cell area: A = 0.033 cm², B = 0.16 cm²
AM1, 100 mW/cm² at 25 °C

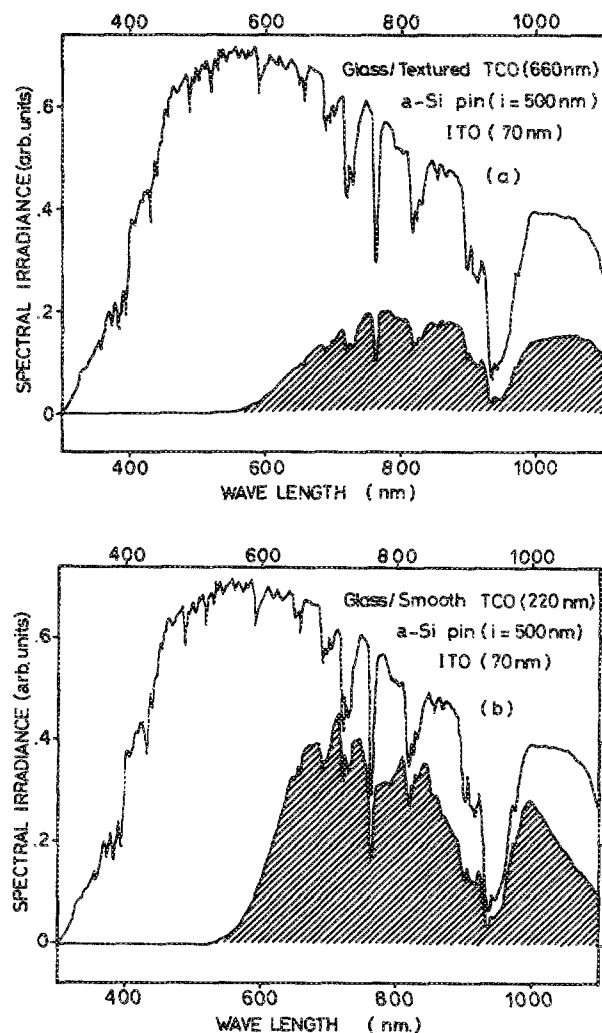


FIG. 9. Solar spectral irradiance and their transmitted light spectra through a -Si solar cell fabricated on (a) a textured glass substrate and (b) a smooth glass substrate.

est conversion efficiency of 16.8% in this work. This value represents one of the highest efficiencies reported so far in a wide variety of a -Si-based solar cells including a -Si/crystalline-Si and a -Si/CIS (copper indium selenium-2) tandem-type solar cells.

VI. SUMMARY

A new type of high-efficiency solar cell has been developed by a simple production process with only a electron cyclotron resonance plasma CVD of highly conductive microcrystalline silicon carbide under a low-temperature process. The ECR plasma CVD system has dynamic properties to produce the microcrystalline phase, and so the material exhibits excellent controllability of the electrical properties

by impurity doping. The optical band gap of μc -SiC:H can be varied over a large range, from 2.1 to 2.7 eV, while retaining good electrical conductivity.

Outstanding features of p -type μc -SiC:H satisfy the essential requirements for a wide-gap window material in heterojunction solar cells. The development of a simple structure and simple process sequence of heterojunction solar cells with deposition of this microcrystalline materials demonstrates a large short-circuit current density as well as excellent heterojunction properties on the polycrystalline silicon substrate. The best efficiency reached is 15.4% in a single-heterojunction device.

The experimental approaches for higher-efficiency tandem-type solar cells have revealed the importance of the use and selection of proper materials for each operation condition. In this stage, we have achieved 16.8% conversion efficiency in a -Si/poly-Si four-terminal tandem-type solar cells.

ACKNOWLEDGMENTS

The authors are grateful to Osaka Titanium Co. for the supply of cast polycrystalline silicon substrate. This work is partially supported by the Sunshine project in contract with the New Energy Development Organization of the Ministry of International Trade and Industry.

- ¹ J. L. Stone, in Proceedings of the 4th International Photovoltaic Science and Engineering Conference, Sydney, Australia, February 1989, p. 19.
- ² C. R. Wronski, in *Semiconductors and Semimetals, Hydrogenated Amorphous Silicon*, edited by J. I. Pankove (Academic, New York, 1984), Vol. 21, Pt. C, p. 347.
- ³ S. Nakano, T. Takahama, M. Isomura, M. Nishikuni, K. Watanabe, N. Nakamura, S. Tsuda, M. Ohnishi, Y. Kishi, and Y. Kuwano, in Proceedings of the 2nd International Photovoltaic Science and Engineering Conference, Beijing, August 1986, p. 483.
- ⁴ Y. Hattori, D. Kruangam, K. Ktoh, Y. Nitta, H. Okamoto, and Y. Hamakawa, in Proceedings of the 19th IEEE Photovoltaic Specialists Conference, New Orleans, May 1987, p. 689.
- ⁵ H. Takakura, Y. Matsumoto, K. Miyagi, G. Hirata, T. Kanata, H. Okamoto, and Y. Hamakawa, in Proceedings of the International Solar Energy Society, Solar World Congress, Kobe, September 1989 (to be published).
- ⁶ Y. Hattori, D. Kruangam, T. Toyama, H. Okamoto, and Y. Hamakawa, *Appl. Surf. Sci.* **33/34**, 1276 (1988).
- ⁷ D. Kruangam, T. Toyama, Y. Hattori, M. Deguchi, H. Okamoto, and Y. Hamakawa, *J. Non-Cryst. Solids* **97/98**, 293 (1987).
- ⁸ M. Matsuoka and K. Ono, *J. Vac. Sci Technol. A* **6-1**, 25 (1988).
- ⁹ G. D. Cody, in *Semiconductors and Semimetals, Hydrogenated Amorphous Silicon*, edited by J. I. Pankove (Academic, New York, 1984), Vol. 21, Pt. B, p. 11.
- ¹⁰ Y. Hamakawa, Y. Matsumoto, G. Hirata, and H. Okamoto, in Proceedings of Materials Research Society Symposia, Boston, November 1989 (to be published).
- ¹¹ H. Fujioka, M. Itoh, and K. Takasaki, in Proceedings of the Materials Research Society Symposia, Boston, November 1989 (to be published).